

Dalton Transactions

Accepted Manuscript

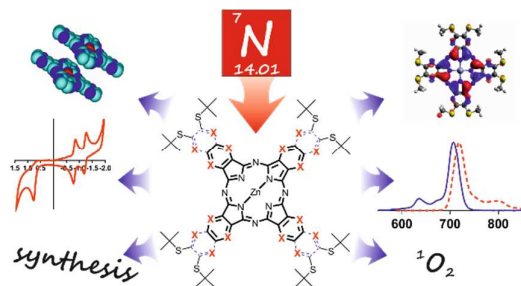


This is an *Accepted Manuscript*, which has been through the Royal Society of Chemistry peer review process and has been accepted for publication.

Accepted Manuscripts are published online shortly after acceptance, before technical editing, formatting and proof reading. Using this free service, authors can make their results available to the community, in citable form, before we publish the edited article. We will replace this *Accepted Manuscript* with the edited and formatted *Advance Article* as soon as it is available.

You can find more information about *Accepted Manuscripts* in the [Information for Authors](#).

Please note that technical editing may introduce minor changes to the text and/or graphics, which may alter content. The journal's standard [Terms & Conditions](#) and the [Ethical guidelines](#) still apply. In no event shall the Royal Society of Chemistry be held responsible for any errors or omissions in this *Accepted Manuscript* or any consequences arising from the use of any information it contains.



Series of phthalocyanines, naphthalocyanines and their aza-analogs were studied and compared using UV-vis and MCD spectra, molecular calculations, photophysical and electrochemical measurements.



Journal Name

ARTICLE

Systematic investigation of phthalocyanines, naphthalocyanines, and their aza-analogues. Effect of the isosteric aza-replacement in the core.

Received 00th January 20xx,
Accepted 00th January 20xx

DOI: 10.1039/x0xx00000x

www.rsc.org/

Veronika Novakova,^{*a} Petra Reimerova,^a Jan Svec,^b Daniel Suchan,^b Miroslav Miletin,^b Hannah M. Rhoda,^c Victor N. Nemykin^{*c} and Petr Zimcik^{*b}

A series of zinc complexes of phthalocyanine, naphthalocyanine and their aza-analogues with alkylsulfanyl substituents was synthesized and characterized by UV-vis and MCD spectroscopy, and their redox properties were investigated using CV, DPV, and SWV approaches as well as spectroelectrochemical methods. Aggregation, photostability, singlet oxygen production, and fluorescence quantum yields of the target complexes were studied as a function of the stepwise substitution of the aromatic C-H fragments by nitrogen atoms. The electronic structure and vertical excitation energies of the target compounds were probed by DFT-PCM and TDDFT-PCM approaches. Introduction of additional nitrogens into the structure leads to a hypsochromic shift of the Q-band and makes the macrocycle strongly electron deficient and more photostable. The impact on the photophysics is limited. The relationships between the type of macrocycle and the studied properties were defined.

Introduction

Phthalocyanines (Pcs) are synthetic macrocyclic dyes with structural similarities to naturally occurring porphyrins. Since their first synthesis in 1907, they have attracted steady attention in a number of areas, together with their aza-analogues (azaphthalocyanines) or homologues with an enlarged macrocyclic system (e.g., naphthalocyanines, Ncs).¹ Strong absorption in the red part of the visible spectrum imparts them with blue to green color; thus, Pcs are produced in tens of thousands of tons per year as industrial colorants.² However, additional properties of these chemically and thermally stable molecules are highly appreciated. The ability to produce singlet oxygen after irradiation is utilized in the photodynamic treatment (PDT) of tumors³ or in photoactive materials.^{4,5} In addition, strong fluorescence is an advantage in the development of new fluorescent labels⁶ or sensors.⁷ Furthermore, the stacking of the planar macrocyclic ring is ideal for the formation of discotic liquid crystals.⁸ The electron-accepting and electron-donating properties of Pcs have led to

their use in dye-sensitized solar cells (DSSCs),^{9,10} and they are widely studied in electron-transfer processes.¹¹

The properties of Pcs and their analogues or homologues are often optimized for each application. Despite some important reports on structure-activity relationships that mainly consider the influence of peripheral substituents¹² or stepwise enlargement of the macrocyclic system,¹³ detailed studies on isosteric aza-replacement are lacking. The exchange of the methine group in benzene rings for the more electronegative nitrogen atom has been shown to lead to a substantial change in behavior and to new emerging applications for Pc analogues.^{14,15} However, the lack of multifactorial structure-activity relationship data hampers extension of the rational design of Pcs or Ncs to aza-analogues and the tailoring of their properties to selected applications.

This work focuses on the comparison of important properties of Pcs, Ncs and their aza-analogues (Figure 1). Despite a number of reports on Pcs¹⁶, Ncs¹⁷ and tetrapyrroloporphyrins (TPyzPzs)¹⁸, information about other aza-analogues containing pyrazine rings – tetra(2,3-quinoxalino)porphyrins (2,3-TQPzs)¹⁹, tetra(6,7-quinoxalino)porphyrins (6,7-TQPzs)^{20,21} and tetra(pyrazinopyrazino)porphyrins (TPyzPyzPzs) – are scarcely found in the literature. In particular, for TPyzPyzPzs, only one report can be found in peer-reviewed journals.²² Moreover, a systematic investigation of Pc and Nc aza-analogues with electron-donating groups has not yet been conducted. Thus, this study aims to investigate the impact of the isosteric replacement of CH by N in benzene rings in Pcs and Ncs on the synthesis, absorption and emission spectra, fluorescence and singlet oxygen quantum yields, solubility,

^aDepartment of Biophysics and Physical Chemistry, Faculty of Pharmacy in Hradec Kralove, Charles University in Prague, Heyrovskeho 1203, 50005, Hradec Kralove, Czech Republic, veronika.novakova@faf.cuni.cz

^bDepartment of Pharmaceutical Chemistry and Drug Control, Faculty of Pharmacy in Hradec Kralove, Charles University in Prague, Heyrovskeho 1203, 50005, Hradec Kralove, Czech Republic, zimcik@faf.cuni.cz

^cDepartment of Chemistry & Biochemistry, University of Minnesota Duluth, 1039 University Drive, Duluth, MN 55812, USA, vnykyin@d.umn.edu

† Footnotes relating to the title and/or authors should appear here.

Electronic Supplementary Information (ESI) available: experimental details, NMR spectra, figures with details on absorption spectra, solubility, aggregation, photophysics, photostability, electrochemistry, predicted parameters for target compounds. See DOI: 10.1039/x0xx00000x

aggregation, and electrochemical properties of these compounds. These parameters all play an important role in the development of new candidates for PDT, fluorescent probes, sensors, liquid crystals, DSSCs, and many other applications. The structure of the studied compounds was fixed from the perspective of the central metal and peripheral substituents to observe changes that are attributable to the macrocyclic core only. Bulky *StBu* substituents were selected as the most appropriate groups because they limit aggregation that may negatively influence the determination of photophysical parameters (singlet oxygen and fluorescence quantum yields) and thus lead to misleading conclusions. For the purposes of this article, abbreviations of the macrocycles that are written in bold (e.g., **TPyzPz**) refer to a particular compound as drawn in Figure 1. Abbreviations that are written normally (e.g., TPyzPz) represent the macrocycle type with no particular peripheral substitution or central cation.

Figure 1

Figure 1. Structures of the investigated compounds.

Results and Discussion

Synthesis

Aromatic *ortho* dicarbonitriles are typical precursors for the synthesis of Pcs and related compounds.^{16, 23} For heteroatom-substituted dicarbonitriles, nucleophilic substitution of activated aromatic dicarbonitriles is the pathway of choice for their synthesis in many reported cases.²⁴ Nucleophilic substitution (Scheme 1) leading to compounds **1-5** reflected well the electron-deficient properties of carbons next to the halogens. The yields for the more electron-deficient derivatives **1-4** were typically over 70 % when the reaction was performed with equimolar ratios and at room temperature. The reaction ran well even in the presence of water in case of **1-3**. In contrast, very low sensitivity of the naphthalene derivative towards nucleophiles required the heating of 6,7-dibromonaphthalene-2,3-dicarbonitrile with a large excess of thiolate to produce compound **5** with a moderate yield of 51 %. Approximately the same electron-deficient properties of the carbons in positions 2,3 and 6,7 in 6,7-dibromoquinoline-2,3-dicarbonitrile complicated the synthesis of precursor **6**. Nucleophilic substitution with *tert*-butylthiolate gave an inseparable mixture of quinoxalines with CN or Br exchanged for *StBu*. A reverse approach that leads to the introduction of *StBu* to the aromatic core first and carbonitriles in the final step was therefore developed. The published procedure for 4,5-bis(*tert*-butylsulfanyl)benzene-1,2-diamine (**7**) was optimized (see Electronic Supplementary Information, ESI), leading to the synthesis of this derivative in an overall yield of 50 % based on benzene-1,2-diamine (published overall yield is 10 %²⁵). Subsequent formation of a tetrahydroquinoxaline ring (**8**) from **7** in a reaction with diethyloxalate was followed by chlorination (**9**) and cyanation to obtain precursor **6** (Scheme 1).

Several synthetic methods for the formation of Pcs and analogous macrocycles have been previously developed.²⁶ Two basic approaches of ring formation are based either on initiation of the reaction by alkoxide (original Linstead method) or on a template effect of the metal cation. Both approaches were compared and the data are summarized in Table 1. In summary, the template method using Zn(CH₃COO)₂ in pyridine seems to be advantageous for most types of macrocycles as the yields were generally highest among the compared methods, or at least comparable with the alkoxide approaches. The temperature of the reaction may play a crucial role as the yields of the template methods were often significantly decreased accompanied by the appearance of large amount of dark insoluble product when higher temperatures over 150°C were applied (e.g. using microwave irradiation in closed vessel or reflux in DMF, Table 1).

Table 1. Reaction conditions and corresponding yields for different cyclotetramerization methods^a

Compound	LiOBu ^b	Mg(OBu) ₂ ^c	Zn(CH ₃ COO) ₂ (solvent) ^d
Pc	64%	63%	51 % (pyridine) ^f , 20 % (DMF)
TPyzPz	exchange ^e	41%	61 % (pyridine) ^g , 9 % (DMF)
Nc	30%	30%	10 % (pyridine)
2,3-TQPz	19%	23%	40 % (pyridine)
6,7-TQPz	exchange ^e	12%	43 % (pyridine)
TPyzPyzPz	exchange ^e	exchange ^e	46 % (pyridine), 45 % (DMF)

^aisolated yields, the data are always for final Zn complexes. ^b1. BuOH, Li, reflux, 3 h; 2. Zn(CH₃COO)₂, reflux, 1 h. ^c1. BuOH, Mg, reflux, 12 h; 2. TsOH, THF/chloroform, 2 h, rt; 3. Zn(CH₃COO)₂, pyridine, reflux, 1 h. ^dZn(CH₃COO)₂, anhydr. solvent, argon, reflux, 12 h. ^esome *StBu* substituents were exchanged for OBu. ^f29 % using mw irradiation at 170°C. ^g0 % using mw irradiation at 170°C.

Scheme 1

Scheme 1. Synthesis of precursors.

Figure 2

Figure 2. MCD (upper graph), experimental UV-vis spectra (middle graph) and TDDFT-PCM (lower graph) of **TPyzPz** (A), **TPyzPyzPz** (B), **Pc** (C), **2,3-TQPz** (D), **6,7-TQPz** (E), and **Nc** (F) in pyridine.

In addition to the yield of the reactions, another fact that was also considered is the stability of peripheral chains (*StBu*) under Linstead conditions. It has been reported several times that alkyl/aryl sulfanyl substituents can be exchanged for alkoxide (formed from Li or DBU) used for initiation of the cyclotetramerization reaction in the case of electron-deficient macrocycles such as TPyzPzs.²⁷ This was also observed for compounds in our studied series bearing pyrazine as the outer ring (**TPyzPz**, **6,7-TQPz**, and **TPyzPyzPz**) when using a LiOBu initiator. No exchange of peripheral substituents (besides **TPyzPyzPz**) was observed when using a Mg(OBu)₂ initiator that previously proved to be a mild cyclotetramerization agent.²⁸ However, mass spectra of a **TPyzPyzPz** sample from the Mg(OBu)₂ reaction revealed substantial exchange of peripheral



Journal Name

ARTICLE

Table 2. UV-vis absorption and photophysical data of the studied compounds.^a

	TPyzPz		TPyzPyzPz		Pc		2,3-TQPz		6,7-TQPz		Nc	
	THF	Pyridine	THF	Pyridine	THF	Pyridine	THF	Pyridine	THF	Pyridine	THF	Pyridine
λ_{\max} [nm]	650	657	693	705	699	707	716	731	744	754	773	786
log ϵ	5.48	5.44	5.41	5.45	5.52	5.45	5.52	5.54	5.64	5.66	5.63	5.63
λ_f [nm]	657	663	700	712	709	718	722	738	749	760	781	793
$\Delta\lambda$ [nm]	7	6	7	7	10	11	8	7	5	6	8	5
Φ_f	0.30	0.27	0.19	0.17	0.28	0.24	0.17	0.20	0.18	0.23	0.19	0.18
Φ_A	0.62	0.65	0.68	0.70	0.65	0.63	0.62	0.67	0.59	0.63	0.56	0.58
$\Phi_f + \Phi_A$	0.92	0.92	0.87	0.87	0.93	0.87	0.79	0.87	0.77	0.86	0.75	0.76
Photostability (%) ^b	-	96	-	85	-	93	-	82	-	68	-	43

^a λ_{\max} (absorption maximum in the Q-band), ϵ (extinction coefficient at λ_{\max}), λ_f (fluorescence emission maximum), $\Delta\lambda$ (Stokes shift), Φ_f (fluorescence quantum yield), Φ_A (singlet oxygen quantum yield). ^bExpressed as % of the compound remained unchanged after irradiation of $\sim 2 \mu\text{M}$ solution with 400 W lamp for 30 min. Photostability of ZnPc under the same conditions = 91 %.

StBu for OBU substituents. It seems that the strongly electron-deficient pyrazinopyrazine moiety in **2** (see also results from cyclic voltammetry) increased the partial positive charge on carbons 6 and 7 and allowed efficient attack of this site even by the mild magnesium butoxide. For this reason, only template methods can be applied for the successful synthesis TPyzPyzPz. On the other hand, mass spectra indicated full stability of the peripheral substituents of TPyzPz or 6,7-TQPz in Mg(OBU)₂ or for Pc, Nc, and 2,3-TQPz even in LiOBU.

UV-vis and MCD spectra

UV-vis and MCD spectra of the target complexes in pyridine are presented in Figure 2. It was found that all compounds are present in monomeric form in both THF and pyridine (see also Figure S7) in the concentrations range typical for optical spectroscopy (up to 5 μM). In all cases, typical for Pcs and their analogues,²⁹ strong Q-band and its vibronic satellites were observed in the low-energy region of the spectra. Its energy varies between 657 and 786 nm and this excited state degeneracy was further confirmed by clear Faraday A-terms observed in corresponding MCD spectra. Indeed, all of Faraday A-terms are centered close to the absorption Q-band maxima of corresponding zinc complexes. As expected,^{16, 23} introduction of eight StBu substituents into β -positions of the Pc or Nc macrocycle resulted in ~ 20 -40 nm low-energy shift of the Q-band compared to their unsubstituted analogues (Table 2). Isosteric replacement of aromatic C-H fragments with nitrogen atoms in all cases caused a hypsochromic shift of the Q-band. For instance, this shift is ca 50 nm when going from Pc to TPyzPz. Similarly, Nc complex has the lowest energy Q-band when compared with the 6,7-TQPz, 2,3-TQPz, and TPyzPyzPz aza-analogues. Although the largest energy shift of Q-band is expected and experimentally was observed (81 nm) for TPyzPyzPz (a macrocycle with the highest degree of nitrogen

substitution), the high-energy Q-band shift in 6,7-TQPz and 2,3-TQPz complexes is rather instructive (Figure 2). Indeed, when the outer benzene ring accommodates two nitrogen atoms (6,7-TQPz complex), the Q-band undergoes only 34 nm higher energy shift, while in the case of inner benzene ring replacement (2,3-TQPz complex) much larger (55 nm) high-energy Q-band shift was observed. These results are in good agreement with the observations of Kobayashi et al. who studied a series of enlarged porphyrazines,¹³ and our previous observations of a linear shift of the Q-band position in asymmetric TPyzPzs/6,7-TQPzs.²¹ The results are also in line with those obtained recently by Donzello and co-workers for Mg complexes of octapyridinated TPyzPz and octapyridinated 6,7-TQPz.³⁰ The red shift of 101 nm between these two reported homologues in DMF compares well with 97 nm between TPyzPz and 6,7-TQPz in pyridine. A general trend of an increasing extinction coefficient with a low-energy shift of the Q-band was also observed (Table 2, Figure S7). Interestingly, the extinction coefficient reached very high values over 400 000 $\text{M}^{-1} \text{cm}^{-1}$ for 6,7-TQPz and Nc which is in accordance with data for this type of macrocycles when they are not aggregated.³¹

In addition to the Q-band, classic B- (Soret) band was observed in UV-vis spectra of all target complexes between 368 and 405 nm (Figure 2). Similar to the other Pcs and their analogues,³² this band is associated with ~ 10 times weaker Faraday A-term in MCD spectra of zinc complexes, which are centered close to the corresponding UV-vis maxima. The energy of the B-band, however, follows opposite trend as compared to the energy of the Q-band, i.e. it undergoes low-energy shift upon stepwise substitution with the nitrogen atoms. For instance, based on position of MCD A-terms, B-band is observed at 359 nm in Nc, 370 nm in Pc, 380 nm in TPyzPz, 385 nm in 6,7-TQPz and 2,3-TQPz, and 389 in

TPyzPyzPz (a macrocycle with the highest degree of nitrogen groups substitution). In addition to the B-band, all aza-analogues have an additional

----- Figure 3 -----

Figure 3. DFT-PCM predicted orbital energy diagram for target compounds. (A) Frontier orbital energies; (B) selected orbital energies for most important orbitals

band in 400 - 500 nm region, which is present as a weak shoulder in UV-vis spectra of the parent **Pc** and **Nc** complexes (Figure 2). This band is associated with very weak MCD signals with exception of **TPyzPyzPz** complex in which it is correlated with a relatively strong negative MCD signal.

DFT and TDDFT calculations

The electronic structures and vertical excitation energies of octaalkylsulfanyl **Pc**, **Nc**, and their aza-analogues were probed by DFT and TDDFT approaches. In order to correlate DFT and TDDFT data with experimental UV-vis spectra and redox properties, polarized continuum model (PCM) approach and pyridine solvent were used in all calculations. DFT-PCM predicted frontier orbitals compositions are listed in Table S4, the orbital energy diagram is shown in Figure 3, and selected molecular orbitals (MO) profiles are depicted in Figure 4 and Figure S18. In all tested compounds, the HOMO has a_{1u} symmetry and resembles classic Gouterman's MO³³ with a large contribution from the α - and β -pyrrolic carbons in a respective macrocycle complimented by an appreciable contribution from the peripheral atoms of sulfur (Figure 4). It should be noted that the similar significant contribution into HOMO from the electron-donating alkoxy and alkylsulfanyl substituents was observed earlier by Kobayashi and co-workers.¹² The energy of a_{1u} HOMO correlates very well with the experimental first oxidation potential (for electrochemical data see Table 3 and discussion below) for target systems (Figure S19) and in general gets more stable with the increase of the number of nitrogen atoms in respective macrocycle (Figure 3). When direct comparison is possible (**TPyzPyzPz**, **2,3-TQPz**, and **6,7-TQPz** complexes) introduction of the nitrogen atoms in the inner benzene fragment provides significantly larger stabilization of the HOMO energy compared to the substitution of the outer benzene fragment with the same number of the nitrogen atoms. The LUMO and LUMO+1 also resemble classic Gouterman's e_g pair which is dominated by contribution not only from the α - and β -pyrrolic carbon atoms, but also from *meso*- and inner nitrogen atoms (Figure 4). The energies of LUMO and LUMO+1 are slightly less sensitive with respect to the substitution of the peripheral benzene fragments with the nitrogen atoms, but roughly follow the same trends as in the corresponding HOMO. Indeed, **TPyzPyzPz** system has the lowest LUMO energy and the energy of LUMO in **2,3-TQPz** is lower than that in **6,7-TQPz** complex. Similarly, good correlation between the energy of LUMO and the first reduction potential was also observed (Figure S20). The situation with the fourth classic Gouterman's orbital of a_{2u} symmetry in all tested complexes is rather interesting. Indeed,

in the case of unsubstituted zinc phthalocyanine,³⁴ the highest energy occupied MO with a_{2u} symmetry is dominated by contributions from *meso*- and inner nitrogen atoms and resembles classic Gouterman's MO. Introduction of eight alkylsulfanyl substituents in our complexes of interest, however, results in a situation, when the highest energy occupied a_{2u} symmetry MO (HOMO-7 in **Nc** and HOMO-4 in all other tested compounds) has very small contribution from the *meso*- and inner nitrogen atoms (Figure 4). In contrary, HOMO-7/HOMO-4 a_{2u} symmetry π -orbital in all tested complexes is dominated by contributions from sulfur atoms and benzene fragments. The classic Gouterman's a_{2u} MO was found to be ~1 eV lower in energy compared to the highest energy a_{2u} orbital in all complexes (Figure 3). Because of the large contribution from the *meso*- and inner nitrogen atoms, this orbital energy follows the general trend observed for the LUMO.

----- Figure 4 -----

Figure 4. Selected DFT-PCM predicted orbitals for target compounds.

According to the classic Gouterman's model,³³ UV-vis spectra of **Pcs** and their analogues could be described to a large extent in the borders of "four-orbital" model, which involves different degrees of configuration interaction between single-electron excitations originating from a_{1u} (HOMO), a_{2u} (HOMO-1), and e_g (LUMO, LUMO+1) orbitals. In particular, in this model, low-energy (~2 eV) Q-band should be dominated by $a_{1u} \rightarrow e_g$ contribution, while B-band region should predominantly originate from $a_{2u} \rightarrow e_g$ excitations. In our case, classic Gouterman's a_{2u} MO is not the highest energy occupied orbital of a_{2u} symmetry. DFT-PCM calculations predict another occupied a_{2u} symmetry MO with ~1 eV energy higher than the classic Gouterman's a_{2u} MO. It could be expected²³ that this MO will have high energy only in the case of **Pcs**, **Ncs**, and their aza-analogues with electron-donating substituents and thus, it is not surprising that it was not mentioned earlier for the aza-analogues of **Pcs** and **Ncs** with electron-withdrawing groups. As a result, one might expect an appearance of the additional intense absorption bands with the energies between Q- and B-bands. Thus, in order to correlate experimental UV-vis spectra of the target zinc complexes and assign an experimentally observed unusual intense bands in 450 - 500 nm region, we conducted a set of TDDFT-PCM calculations, which proven to provide a very good agreement between the energies of experimental and theoretical vertical transitions in a number of **Pcs** and their analogues.^{30, 34, 35} TDDFT-PCM predicted UV-vis spectra of the target zinc complexes correlated very well with the experimental data both in terms of energies and intensities (see Figure 2 for nm scale and Figure S23 for cm^{-1} scale data). First, TDDFT-PCM calculations suggest that the Q-band region should originate from two degenerate excited states (states 1 and 2, Table S3), which is dominated by a_{1u} (HOMO) $\rightarrow e_g$ (LUMO, LUMO+1) single-electron contributions. Predicted theoretical energies are in excellent agreement with the experimental values (Figure S21) and indicative of the lowest

Q-band energy for **Nc** and the highest Q-band energy for **TPyzPz**. Second, in agreement with their electronic structure, bands in the $\sim 450 - 500$ nm region were found to be dominated by the pair of doubly degenerate transitions, which have predominant a_{2u} (HOMO-7/HOMO-4) $\rightarrow e_g$ (LUMO, LUMO+1) character (Table S3). Again, an excellent correlation between the TDDFT-PCM predicted and experimentally observed energies for $\sim 450 - 500$ nm region has been observed (Figure S22). In addition, clear correlation can be seen also for the TDDFT-PCM predicted oscillator strengths and experimentally observed intensities (Figure 2). Finally, according to TDDFT-PCM calculations, B-band region can be described by several excited states with two of them dominated by the Gouterman's $a_{2u} \rightarrow e_g$ single-electron excitations (Table S3). Thus, TDDFT-PCM calculations on the target zinc complexes correlate very well with their electronic structure and clearly indicate that the major contribution into the UV-vis spectra in $\sim 450 - 500$ nm region should originate from the a_{2u} (HOMO-7/HOMO-4) $\rightarrow e_g$ (LUMO, LUMO+1) excitations with a_{2u} symmetry MO being delocalized over sulfur atoms and benzene fragments of corresponding macrocycles.

----- Figure 5 -----

Figure 5. Changes in the absorption spectra of **TPyzPz** (A) and **TPyzPzPz** (B) in toluene upon dilution from 100 μM (red spectrum) to 0.125 μM (blue spectrum). Inset A: dependence of ϵ at 654 nm on the concentration in toluene. Inset B: fluorescence emission spectra of **TPyzPzPz** in toluene with emission of monomer and J-dimer (red) and pyridine with monomer only (black). The spectra were normalized to the same fluorescence intensity of monomeric species.

Aggregation

Planar macrocyclic cores of **Pc** and analogues tend to aggregate due to $\pi-\pi$ interactions. This may allow formation of compounds with interesting liquid crystalline properties³⁶ or on the other hand may reduce usability in applications connected with photophysical processes upon photon absorption due to formation of face-to-face aggregates of the H-type.³⁷ However, J-aggregates with highly interesting photophysical behavior were also reported for **Pcs** substituted with coordinating peripheral substituents.^{11, 38, 39}

Aggregation of the target compounds was compared in toluene due to high solubility of most of the studied compounds (for solubility study see ESI) and the non-coordinating character of this solvent. Compound **2,3-TQPz** was not studied, as it was insoluble in toluene. Aggregation was observed in all cases at high concentrations (close to 100 μM) as indicated by the decrease of the extinction coefficient of the Q-band and broadening of the spectra (Figure 5a, Figure S9). The changes suggested formation of H-type aggregates in most cases besides **TPyzPzPz** with atypical behavior (see below). Increase in the Q-band extinction coefficient and sharpening of the spectra was observed upon dilution. Appearance of several isosbestic points in several cases indicated the transformation of dimers to monomers. The strongest aggregation was detected for **Nc** with $K_D = 3.3 \times 10^5$

M^{-1} . Extensive aggregation of **TPyzPz**, **Pc** and **6,7-TQPz** appeared at very high concentrations only (over the detection limit of the instrument even with 1 mm pathlength cuvettes), which did not allow the exact determination of K_D values. Based on rough analysis of the data (Figure S9), the K_D values are estimated to be approximately $1.0 \times 10^4 \text{ M}^{-1}$ or lower for these three compounds. No unequivocal conclusion on the influence of the macrocycle type and size on K_D can be made from the determined values, although smaller macrocycles (**Pc** and **TPyzPz**) seem to be less susceptible to dimerization than the enlarged ones.

A strategy of introduction of eight bulky *t*Bu substituents for reduction of the aggregation seems to be efficient as $K_D \leq 1.0 \times 10^4 \text{ M}^{-1}$ for **Pc** is lower than for zinc tetra(*tert*-butyl)phthalocyanine ($K_D = 2.5 \times 10^4 \text{ M}^{-1}$ in toluene)⁴⁰ or for octakis(3,7-dimethyloctyloxy)phthalocyanine ($K_D = 1.5 \times 10^6 \text{ M}^{-1}$ in dodecane). Furthermore, although reported $K_D = 2.72 \times 10^5 \text{ M}^{-1}$ (in THF) for zinc octakis(3,6-dioxa-1-decylthio)naphthalocyanine⁴¹ is slightly lower than for **Nc** ($K_D = 3.3 \times 10^5 \text{ M}^{-1}$ in toluene) it must be kept in mind that it has been determined in THF that strongly reduces aggregation.

Extremely high aggregation was observed for **TPyzPzPz**, which was found aggregated in toluene even at the lowest tested concentration of 0.125 μM (Figure 5b). This behavior did not allow determination of its dimerization constant (K_D), which is far above $2.0 \times 10^7 \text{ M}^{-1}$. Interestingly, the absorption spectra with well pronounced red-shifted band indicated formation of J-dimer together with presence of residual monomer. This fact is supported by extraordinarily high K_D which is in accordance with the typical $K_D \cong 1 \times 10^{11} \text{ M}^{-1}$ for J-dimers of **Pcs**.^{11, 38} Fluorescence emission spectra of **TPyzPzPz** in toluene were subsequently collected and indeed, the emission band of monomer was accompanied by another red shifted band ($\lambda_{\text{em}} = 784$ nm, Figure 5b, inset) that is typical for presence of J-dimers.³⁹ Fluorescence excitation spectra measured at different emission wavelengths further confirmed presence of two fluorescent species in the sample (Figure S10). All these facts support that **TPyzPzPz** formed stable J-type dimers in toluene most likely on the basis of coordination of one of the pyrazine nitrogens with central zinc cation.

Photophysics and photostability

Photophysical data were obtained in pyridine and THF (Table 2) by the comparative method with unsubstituted **ZnPc** as the reference compound. The emission spectra (Figure 6) mirrored the absorption Q-band shape with a small Stokes shift typically not exceeding 10 nm. The excitation spectra corresponded well to absorption spectra indicating that no aggregation occurred.

Fluorescence quantum yields (Φ_f) of all the studied compounds were comparable with relatively higher Φ_f values for macrocycles, with only four 6-membered aromatic rings annulated to porphyrazine ring. Values for **TPyzPz** and **Pc** were therefore typically above 0.25 while for the other macrocycles they were below 0.20. The highest Φ_f values observed for **TPyzPz** are in good agreement with recent observations of strong fluorescent properties for this type of macrocycle.¹⁴ The

lowest emission wavelength of this strongest fluorescent macrocycle in the presented series also corresponds well to the dependences observed in the series of α - and β -substituted Pcs where Pcs, which exerts emission at shorter wavelengths, had higher Φ_F values.¹²

----- Figure 6 -----

Figure 6. Normalized fluorescence emission spectra of (from left to right) **TPyzPz** (red), **TPyzPyzPz** (orange), **Pc** (green), **2,3-TQPz** (black), **6,7-TQPz** (blue) and **Nc** (magenta) in pyridine.

Singlet oxygen quantum yields (Φ_A) for all of the compounds were close to 0.60, indicating that all are highly efficient in the production of singlet oxygen - an important species in PDT. Notably, quenching of the TPyzPz (or Pc) triplet states by oxygen in organic solvents (and in saturated oxygen) typically approaches 100 %;⁴² therefore, the Φ_A values can serve also as good indicators of intersystem crossing. The sum of Φ_A and Φ_F therefore cover the main deactivation pathways of the excited states. The sum was typically above 0.75, for **Pc** and **TPyzPz** it was over 0.90. The somewhat lower sum of $\Phi_A + \Phi_F$ for larger macrocycles (**Nc**, **6,7-TQP**, **2,3-TQPz**, and **TPyzPyzPz**, see also Figure S11) is most likely a consequence of increased internal conversion of large macrocycles that enabled more efficient collisions with solvent molecules.

----- Figure 7 -----

Figure 7. Photodecomposition of target compounds in pyridine after irradiation with 400 W lamp. **TPyzPz** (full square, red), **Pc** (full triangle with black border, green), unsubstituted ZnPc (asterisk, black dashed line), **TPyzPyzPz** (open square, orange), **2,3-TQPz** (open triangle, black), **6,7-TQPz** (full circle, blue), **Nc** (open circle, magenta).

Pcs and related macrocycles are known to undergo a photodecomposition upon irradiation with light.⁴³ Rate of the decomposition can be, however, influenced by structural factors, e.g. perfluorination of the peripheral substituents was recently found to substantially increase the photostability.⁴ The photostability of the target compounds was tested in pyridine and compared with that of unsubstituted ZnPc. Irradiation of the solution of the tested compound led to decrease in absorption in all wavelengths from 350 to 900 nm (Figure S12). No new bands were detected. It may lead to conclusion that the whole macrocycle is decomposed to small parts, most likely homologues and analogues of isoindole similarly as observed previously.⁴⁴ The photostability (Table 2, Figure 7) substantially decreased with enlargement of the conjugated system with **Nc** being the least photostable macrocycle. At the same time, a marked trend in increasing photostability with nitrogen substitution can be traced. Thus, the photostability of **Nc** increased by nitrogen substitution in order **6,7-TQPz** < **2,3-TQPz** < **TPyzPyzPz**. Similarly, **TPyzPz** was more photostable than **Pc** and, in fact, the least susceptible to decomposition by light among the target compounds. All the data corresponded well with correlations reported by Wöhrl

et al.⁴⁴ for photostability of unsubstituted zinc Pc, TPyzPz and Nc.

----- Figure 8 -----

Figure 8. Cyclic voltammograms (pyridine, 100 mV/s, 0.1 M tetrabutylammonium hexafluorophosphate, 25 °C) of **TPyzPyzPz** (orange), **2,3-TQPz** (black), **TPyzPz** (red), **Pc** (green), **6,7-TQPz** (blue) and **Nc** (magenta).

Electrochemistry and spectroelectrochemistry

The electrochemistry of the studied macrocycles was assessed *via* cyclic voltammetry, differential pulse voltammetry and square-wave voltammetry (Figures S13, S14) in THF and pyridine at room temperature with ferrocene as an internal standard. Cyclic voltammograms are shown in Figure 8. Half-wave potentials were determined by square wave voltammetry and are listed in the Table 3. All compounds in the series underwent at least two reversible reductions in the electrochemical window provided by the solvents, with **TPyzPyzPz** and **2,3-TQP** (the most electron-deficient ones) even undergoing four reductions in the electrochemical window of pyridine and THF. Similarly, four or even five one-electron reductions were described in the literature for remarkably electron-deficient metal complexes of octapyridinated TPyzPz.⁴⁵ Chemical reversibility of the reductions was clearly obvious from the peak current ratios i_{pa}/i_{pc} being close to one at all scan rates. Further, electrochemical reversibility of the reduction processes was assigned on the bases of independency of E_{pa} and E_{pc} on the scan rate (50 mV/s, 100mV/s and 200mV/s; data not shown). Electrochemical reversibility can be deduced also from the peak potential separation (ΔE_p) which was lower than 78 mV (for all compounds of the series). Such value indicates that one-electron processes took place that is also in accordance with the data obtained from spectroelectrochemistry (see below).

In agreement with previous reports on TPyzPz,⁴⁶ the current results showed that pyrazine rings condensed directly to the porphyrine ring strengthened significantly the electron-deficient character of the macrocycle, as characterized by the position of the first reduction potential (E_{red}^1). Thus, the first reduction of **TPyzPyzPz** in pyridine was observed at -0.49 V vs. SCE followed by **2,3-TQP** and **TPyzPz**, which reached values of -0.56 and -0.70 V vs. SCE in pyridine, respectively. Annelation of the pyrazine ring externally to the Pc core does not influence the reduction potential so much and **6,7-TQPz** had even more negative first reduction potential (-0.92 V) than **Pc** itself (-0.81 V). In general, the feasibility of the macrocycle to undergo reduction (i.e., electron-deficient properties) increases in the series **Nc** < **6,7-TQPz** < **Pc** < **TPyzPz** < **2,3-TQPz** < **TPyzPyzPz** (Figure S16).

In contrast to reversible reduction processes, chemically irreversible oxidations (i_{pa} was several times higher than i_{pc}) were observed within the whole series. Such irreversibility of the first oxidation process in all complexes can be explained by



Journal Name

ARTICLE

Table 3. Electrochemical data of target compounds in THF and pyridine.^a

	TPyzPz		TPyzPyzPz		Pc		2,3-TQPz		6,7-TQPz		Nc	
	THF	Pyridine	THF	Pyridine	THF	Pyridine	THF	Pyridine	THF	Pyridine	THF	Pyridine
E_{ox}^1 (V)	1.07	1.05	1.15	1.15	0.80	0.74	0.98	1.02	0.58	0.57	0.40	0.35
E_{red}^1 (V)	-0.76	-0.70	-0.49	-0.49	-0.85	-0.81	-0.66	-0.56	-0.93	-0.92	-1.15	-0.97
E_{red}^2 (V)	-1.12	-1.08	-0.79	-0.81	-1.06	-1.23	-0.98	-0.88	-1.06	-1.30	-1.54	-1.35
E_{red}^3 (V)			-1.20	-1.19			-1.18	-1.17				
E_{red}^4 (V)			-1.44	-1.42			-1.48	-1.38				
HOMO (eV)	-5.49	-5.47	-5.57	-5.57	-5.22	-5.16	-5.40	-5.44	-5.00	-4.99	-4.82	-4.77
LUMO (eV)	-3.57	-3.73	-3.93	-3.94	-3.57	-3.61	-3.76	-3.86	-3.49	-3.50	-3.27	-3.45
λ_{max} [nm]	650	657	693	705	699	707	716	731	744	754	773	786

^aPotentials E_{red} and E_{ox} are expressed as $E_{1/2}$ (in V vs. SCE) with ferrocene as internal standard.

Figure 9

Figure 9. Spectroelectrochemical transformation of the neutral **Pc** (left, A, C) and **TPyzPz** (right, B, D) complexes during the first (A, B) and the second (C, D) reductions in pyridine/TBAP system.

significant contribution of the sulfur atoms in the HOMO as predicted by DFT calculations. Indeed, formation of the radical-cation upon oxidation would result in a system with significant sulfur-centered radical character, which is expected to undergo irreversible chemical transformation in solution. Due to very weak i_{pc} (see Figure 8), the half-wave oxidation potentials (E_{ox} , Table 3) were determined using square-wave voltammetry where the signal of oxidation was clearly observable. The oxidation potentials followed the opposite trend than reduction, i.e., from 0.35 V vs. SCE (for **Nc**) up to 1.15 V. vs. SCE (for **TPyzPyzPz**). The HOMO-LUMO gap calculated from the electrochemical data decreased linearly with the increasing position of Q-band maximum (see Figure S15) in accordance with theoretical predictions.

In order to clarify the nature of the redox-generated species in the target complexes, spectroelectrochemical experiments in pyridine/TBAP system were conducted (Figure 9 and Figure S17). Since the first oxidation process in all studied complexes is irreversible, only reduced species were investigated. Moreover, because of the degradation of mono-anions of larger macrocycles (**Nc**, **6,7-TQPz**, **2,3-TQPz**, and **TPyzPyzPz**) during second reduction process, only data for the first reduction in these systems are presented. In the case of smaller macrocycles **Pc** and **TPyzPz**, during the first reduction, intensities of both Q- and B-band decreased, while formation of three new bands in NIR region between 750 and 1000 nm was clearly observed (Figure 9). In addition, two new bands in

visible regions around 560-600 and 435-440 nm were also observed. Considering the electrochemically inactive central zinc(II) cation and theoretical and spectroelectrochemical data reported in literature, such transformation is very characteristic and indicative of formation of a single-electron reduced macrocycle.^{32, 45, 47} During a second reduction process, three NIR bands decayed, while a new prominent band in 535-573 nm region arose in UV-vis spectra of **Pc** and **TPyzPz** complexes (Figure 9), which is, again, indicative of formation of the macrocycle-centered dianion similar to well-known **Pc**-dianions^{32, 47} and **TPyzPz**-dianions.⁴⁵ Similarly to **Pc** and **TPyzPz** complexes, during reduction of larger macrocycles (**Nc**, **6,7-TQPz**, **2,3-TQPz**, and **TPyzPyzPz**), appearance of new NIR bands is indicative of formation of a macrocycle-centered anion-radical species (Figure S17). Thus, in a good agreement with DFT calculations, addition of one or two electrons to doubly degenerate LUMO and LUMO+1 in all studied complexes resulted in formation of the macrocycle-centered reduced species.

Conclusion

The influence of aza-substitution was studied from several points of view. The effect is traceable already on the level of synthesis of precursors (hetero/aromatic dicarbonitriles) during introduction of peripheral substituents by nucleophilic substitution. Presence of nitrogens with higher electronegativity in the structure makes the substitution of halogens by thiolates easier and produces higher yields. As another synthetic consequence, care must be taken in the selection of appropriate cyclotetramerization method. Instead conditions using alkoxide may not be fully suitable for electron-deficient nitrogen heterocycles, in particular those with outer pyrazine rings. A considerable risk of the exchange

of peripheral substituents for alkoxides from the initiator may be reduced by the use of magnesium butoxide, a mild cyclotetramerization agent (for the synthesis of **TPyzPz** or **6,7-TQPz**). In the case of the strongly electron-deficient **TPyzPzPz**, the use of template method is unavoidable, because even magnesium butoxide led to exchange of the peripheral substituents.

From the point of view of the optical spectra, the aza-substitution has a substantial impact on the position of the main Q-band maximum in that it causes a significant high-energy shift. The high-energy shift was found to be highly significant - approximately 50 nm when aza-substitution takes place on the benzene rings attached directly to porphyrine or approximately 30 nm when the exchange is in outer rings. These relationships may be used for rough prediction of the position of the Q-band maximum similar to the case of stepwise insertion of benzene rings into the TPyzPz core in unsymmetrical pyrazino/quinoxalinoporphyrines.²¹

From the point of view of aggregation, no unequivocal conclusions can be made regarding the size of macrocycle or the number and positions of nitrogens. It seems, however, that smaller macrocycles have a lower tendency to aggregate. This conclusion cannot be fully generalized as a low K_D value was also estimated for **6,7-TQPz**. Unexpected formation of J-dimers, most likely on the basis of coordination of one of the pyrazine nitrogens with central metal, was detected for **TPyzPzPz**. No aggregation was detected for any of the studied compounds in THF or pyridine (e.g. during the photophysical experiments).

All macrocycles produced strongly singlet oxygen with Φ_A values typically over 0.60. This is fully sufficient for application to PDT, and all of the macrocycles can be used for the development of new photosensitizers. In this application, conclusions from the aggregation studies and dependences derived for position of the Q-band maximum may be very useful in practical design. Similarly, Φ_F values also did not differ too much within the series, with the strongest fluorescence found for **TPyzPz**. This fact confirmed the findings derived from a smaller series of compounds studied previously¹⁴ and emphasized further the potential of these aza-analogues as promising fluorescent labels. Reversely to limited differences in photophysical behavior, it should be pointed out that aza-substitution substantially increased photostability of the macrocycles. The increased photostability was observed also for smaller macrocycles (**TPyzPz**, **Pc**) when compared to the larger ones (**TPyzPzPz**, **6,7-TQPz**, **2,3-TQPz**, **Nc**).

One of the most significant impacts of aza-substitution was observed in the electrochemical behavior. The presence of pyrazine rings attached directly to the porphyrine core made these macrocycles strongly electron-deficient, with a very low E_{red}^1 value of -0.49 V vs. SCE (in both THF and pyridine) for the most electron-deficient **TPyzPzPz**. The data indicated that macrocycles such as **TPyzPzPz**, **2,3-TQPz**, and **TPyzPz** may find use as electron acceptors in intra/intermolecular electron/charge transfer processes, while **Nc** with a low E_{ox}^1 value of 0.35 V vs. SCE (in pyridine) may be used easily as a

donor in different dyads or triads. Fine tuning of both reduction and oxidation potentials may be further performed using different peripheral substitutions⁴⁸ and central cations as reported previously for **Pc**⁴⁹ or TPyzPz rings.^{13, 45, 50} The great variability of the tuning parameters with known relationships could be used now to rationally design a macrocycle with electrochemical (and photophysical, spectral etc., see above) properties tailored to a desired application. As an example, strongly electron-deficient macrocycles with high fluorescence are required for the development of fluorescent sensors based on intramolecular charge transfer (ICT).⁷ Dyes absorbing at longer wavelengths with limited or no fluorescence in a monomeric state (e.g., as a consequence of non-susceptive ICT) are desired for dark quenchers of fluorescence in DNA hybridization probes.^{15, 51} Moderate electron-deficient properties of the macrocycle together with absorption at longer wavelengths and sufficient production of singlet oxygen are appreciated in pH sensitive photosensitizers in PDT based on photo-induced electron transfer switching between ON and OFF states.⁵² Fine tuning of both oxidation and reduction potentials are needed in DSSCs where the LUMO level of the dye must be sufficiently high in energy for efficient charge injection in the TiO₂ conduction band, and the HOMO level should allow efficient regeneration of the oxidized dye by the electrolyte.⁹

Experimental

General information on the methods and experimental details on UV-vis and MCD spectra, aggregation, photophysical measurements, photostability, electrochemistry, spectroelectrochemistry and theoretical calculations are mentioned in ESI.

Synthesis

Syntheses of precursors **1**⁵³ and **3**⁵⁴ as well as macrocycles **TPyzPz**,⁵⁵ **6,7-TQPz**,⁵⁴ and **Pc**⁵⁵ were published in the literature previously. Alternative approaches to these macrocycles are presented in ESI.

Synthesis of 6,7-bis(tert-butylsulfanyl)pyrazino[2,3-b]pyrazine-2,3-dicarbonitrile (2). 6,7-dichloropyrazino[2,3-b]pyrazine-2,3-dicarbonitrile⁵⁶ (220 mg, 0.88 mmol) was sonicated in THF (15 mL) for 5 min, and the suspension was added all at once into a mixture of 2-methylpropane-2-thiol (158 mg, 200 μ L, 1.75 mmol) in a 1 M aqueous solution of NaOH (1.8 mL, 1.8 mmol). The suspension dissolved immediately, and the reaction was stirred at room temperature (rt) for 1 h. THF was removed under reduced pressure, water was added, and the mixture was washed three times with ethyl acetate. Combined organic layers were dried (Na₂SO₄) and evaporated. The crude product was purified by column chromatography on silica with chloroform as an eluent. The pure sample was recrystallized from methanol to obtain dark yellow crystals (269 mg, 86 %). M.p. slow dec. from 195 °C; ¹H NMR (300 MHz, CDCl₃): δ 1.77 (s, 18H) ppm. ¹³C NMR (75 MHz, CDCl₃): δ 168.4, 142.1, 130.5, 113.1, 53.5, 29.5 ppm. IR (ATR): ν 2963, 2923, 2235, 1543, 1468, 1426, 1364,

1238, 1221, 1161, 1120, 1034, 880 cm^{-1} . Calcd. for $\text{C}_{16}\text{H}_{18}\text{N}_6\text{S}_2$: C 53.61, H 5.06, N 23.44; found: C 53.71, H 5.05, N 22.98 %.

Synthesis of 4,5-bis(tert-butylsulfanyl)phthalonitrile (4). 4,5-Dichlorophthalonitrile (4.9 g, 24.9 mmol, TCI Europe) was dissolved in DMSO (25 mL), and 2-methylpropane-2-thiol (5.6 g, 7 mL, 62 mmol) was added. The mixture was stirred at rt, and finely ground anhydrous K_2CO_3 (13.8 g, 100 mmol) was added in several portions within 1 h. The reaction turned yellow after the first addition of K_2CO_3 . The mixture was stirred at rt for 24 h and then poured into water (200 mL). The white precipitate was collected and recrystallized from methanol to yield white crystals (6.51 g, 86 %). ^1H NMR (300 MHz, CDCl_3): δ 7.85 (s, 2H) and 1.45 (s, 18H) ppm. ^{13}C NMR (75 MHz, CDCl_3): δ 146.9, 136.9, 115.11, 112.4, 49.6, 31.0 ppm. The analytical data corresponded well with those published for this compound previously.⁵³

Synthesis of 6,7-bis(tert-butylsulfanyl)naphthalene-2,3-dicarbonitrile (5). 6,7-Dibromonaphthalene-2,3-dicarbonitrile (700 mg, 2.1 mmol, TCI Europe) was sonicated for 5 min at rt in DMF (40 mL), and 2-methylpropane-2-thiol (2.8 g, 3.5 mL, 31.3 mmol) was added together with 1,8-diazabicyclo[5.4.0]undec-7-ene (DBU, 4.8 g, 4.7 mL, 31.3 mmol). The reaction was heated at 70 °C for 48 h. The solvent was partially removed under reduced pressure, and the residue was poured into water (50 mL). The suspension was washed three times with ethyl acetate and purified by column chromatography on silica with hexane/ethyl acetate (6:1) as an eluent. The pure sample was recrystallized from ethanol to obtain yellow crystals (377 mg, 51 %). M.p. 191.6–192.0 °C. ^1H NMR (300 MHz, CDCl_3): δ 8.25 (s, 2H), 8.11 (s, 2H), 1.46 (s, 18H) ppm. ^{13}C NMR (75 MHz, CDCl_3): δ 143.7, 134.8, 133.3, 131.5, 115.8, 110.3, 48.8, 31.0 ppm. IR (ATR): ν 2964, 2924, 2235, 1606, 1565, 1458, 1421, 1369, 1346, 1219, 1159, 1090, 981, 927 and 913 cm^{-1} . Calcd. for $\text{C}_{20}\text{H}_{22}\text{N}_4\text{S}_2$: C 67.76, H 6.26, N 7.90; found: C 67.22, H 6.30, N 7.91 %.

Synthesis of 6,7-bis(tert-butylsulfanyl)quinoxaline-2,3-dicarbonitrile (6). Compound **9** (2.9 g, 7.7 mmol, for synthesis of **9** see ESI) was dissolved in DMF (80 mL), and sodium *p*-toluenesulfinate (1.37 g, 7.7 mmol) was added followed by KCN (poison!) (1.15 g, 17.7 mmol). The solution turned deep red after the addition of sodium *p*-toluenesulfinate and subsequently light orange after the addition of KCN. The reaction was stirred overnight at rt. The solvent was removed under reduced pressure, and the residue was purified by column chromatography on silica with toluene/chloroform (2:1) as an eluent to obtain an orange solid (1.7 g, 62 %). M.p. 243.0–245.7 °C (dec.). ^1H NMR (300 MHz, CDCl_3): δ 8.19 (s, 2H), 1.59 (s, 18H) ppm. ^{13}C NMR (75 MHz, CDCl_3): δ 149.7, 139.7, 129.6, 129.2, 113.6, 49.5, 30.7 ppm. IR (ATR): ν 2993, 2973, 2928, 2236, 1573, 1506, 1434, 1372, 1337, 1190, 1162, 1119, 1061, 988, 864 cm^{-1} . Calcd. for $\text{C}_{18}\text{H}_{20}\text{N}_4\text{S}_2$: C 60.64, H 5.65, N 15.72; found: C 60.47, H 5.91, N 15.45 %.

Synthesis of 2,3,11,12,20,21,29,30-octakis(tert-butylsulfanyl)tetrakis(pyrazino[2,3-*b*]pyrazino)porphyrin zinc(II) (TPyzPyzPz). Compound **2** (100 mg, 0.28 mmol) and anhydrous $\text{Zn}(\text{CH}_3\text{COO})_2$ (51 mg, 0.28 mmol) were dissolved in anhydrous pyridine (1 mL) under an

argon atmosphere. The reaction was heated to reflux for 16 h and then poured into water/methanol (1:1 mixture, 100 mL). The precipitate was collected, washed with water, air dried and purified by column chromatography on silica with toluene/pyridine (6:1) as an eluent. After the pure fractions obtained from chromatography were evaporated, the solid was washed thoroughly with methanol to obtain a dark solid (48 mg, 46 %). ^1H NMR (300 MHz, $\text{CDCl}_3/\text{C}_6\text{D}_5\text{N}$ 3:1): δ 1.95 (s, 72H) ppm. ^{13}C NMR (75 MHz, $\text{CDCl}_3/\text{C}_6\text{D}_5\text{N}$ 3:1): δ 163.5, 151.2, 149.8, 143.6, 52.0, 29.9 ppm. IR (ATR): ν 2962, 2922, 1546, 1499, 1359, 1247, 1127, 1063, 1028, 855, 725 cm^{-1} . Calcd. for $\text{C}_{64}\text{H}_{72}\text{N}_{24}\text{S}_8\text{Zn} + 2 \text{H}_2\text{O}$: C 50.07, H 4.99, N 21.90; found: C 50.01, H 5.24, N 21.71 %. UV/Vis (pyridine, 1 μM): λ_{max} (ϵ) 705 (284 300), 669 (38 800), 647 (40 100) 453 (109 800), 405 nm (113 300 $\text{M}^{-1} \text{cm}^{-1}$). MS (MALDI): m/z 1496.3 [M]⁺.

Synthesis of 2,3,11,12,20,21,29,30-octakis(tert-butylsulfanyl)tetra[2,3]quinoxalino)porphyrin zinc(II) (2,3-TQPz). Compound **6** (100 mg, 0.28 mmol) was dissolved in anhydrous butanol (2 mL) and heated to reflux. Lithium metal (2 mg, 0.28 mmol) was added, and the reaction turned dark brown immediately. The reflux continued for 3 h when anhydrous $\text{Zn}(\text{CH}_3\text{COO})_2$ (250 mg, 1.36 mmol) was added. The reaction was refluxed for 1 h and then poured into water/methanol (1:1 mixture, 100 mL). The precipitate was collected, washed with water, air dried and purified by column chromatography on silica with chloroform/pyridine (20:1) as an eluent. After evaporation of the pure fractions obtained from chromatography, the solid was washed thoroughly with methanol to obtain a dark brown solid (22 mg, 21 %). ^1H NMR (300 MHz, $\text{CDCl}_3/\text{C}_6\text{D}_5\text{N}$ 3:1): δ 9.22 (s, 8H), 1.81 (s, 72H) ppm. ^{13}C NMR (75 MHz, $\text{CDCl}_3/\text{C}_6\text{D}_5\text{N}$ 3:1): δ 48.9, 31.2 ppm (aromatic signals were not detected). IR (ATR): ν 2960, 2923, 2856, 1741, 1544, 1432, 1364, 1220, 1158, 1092, 986, 886, 847, 721 cm^{-1} . Calcd. for $\text{C}_{72}\text{H}_{80}\text{N}_{16}\text{S}_8\text{Zn} + 2 \text{H}_2\text{O}$: C 56.62, H 5.54, N 14.67; found: C 56.31, H 5.87, N 14.72 %. UV/Vis (pyridine, 1 μM): λ_{max} (ϵ) 731 (348 800), 695 (46 300), 667 (43 200), 467 (63 400), 394 nm (124 400 $\text{M}^{-1} \text{cm}^{-1}$). MS (MALDI): m/z 1488.1 [M]⁺.

Synthesis of 2,3,11,12,20,21,29,30-octakis(tert-butylsulfanyl)naphthalocyaninato zinc(II) (Nc). Compound **5** (250 mg, 0.7 mmol) and anhydrous $\text{Zn}(\text{CH}_3\text{COO})_2$ (52 mg, 0.28 mmol) were dissolved in anhydrous butanol (5 mL), and 1,8-diazabicyclo[5.4.0]undec-7-ene (DBU, 0.41 g, 0.40 mL, 2.7 mmol) was added. The mixture was heated at reflux for 5 h and then poured into water/methanol (1:1 mixture, 150 mL). The precipitate was collected and washed thoroughly with methanol, hot acetone and cold chloroform. The solid was dissolved in a small amount of pyridine, filtered and dropped into hexane. The precipitate was collected and washed again with hexane, acetone and methanol to obtain a green solid (126 mg, 48 %). ^1H NMR (300 MHz, $\text{C}_6\text{D}_5\text{N}$): δ 9.96 (s, 8H), 9.15 (s, 8H), 1.73 (s, 72H) ppm. ^{13}C NMR (75 MHz, $\text{C}_6\text{D}_5\text{N}$): δ 48.3, 31.4 ppm (aromatic signals were not detected). IR (ATR): ν 2960, 1583, 1455, 1404, 1368, 1333, 1161, 1101, 1084, 1034, 978, 914, 871 cm^{-1} . Calcd. for $\text{C}_{80}\text{H}_{88}\text{N}_8\text{S}_8\text{Zn} + 2 \text{H}_2\text{O}$: C 63.32, H 6.10, N 7.37; found: C 62.94, H 5.96, N 7.35. UV/Vis (pyridine, 1

μM): λ_{max} (ϵ) 786 (423 300), 747 (56 000), 700 (62 800), 362 nm ($102\ 300\ \text{M}^{-1}\ \text{cm}^{-1}$). MS (MALDI): m/z 1480.26 [M]⁺.

Acknowledgements

Veronika Novakova would like to thank Gema de la Torre and Tomas Torres for introduction into the issue of electrochemical measurements, providing equipment and kind guidance. The authors thank Jiří Kuneš for NMR measurements and Juraj Lenčo for MALDI-TOF spectra. The work was supported by the Czech Science Foundation, project no. 13-27761S. The publication is co-financed by the European Social Fund and the state budget of the Czech Republic, project no. CZ.1.07/2.3.00/30.0061. Generous support from Minnesota Supercomputing Institute and U of M Grant-in-Aid to V. Nemykin is greatly appreciated.

Notes and references

- K. M. Kadish, K. M. Smith and R. Guilard, eds., *Handbook of Porphyrin Science*, World Scientific Publishing, Singapore, 2010.
- D. Wöhrle, G. Schnurpfeil, S. G. Makarov, A. Kazarin and O. N. Suvorova, *Macroheterocycles*, 2012, **5**, 191-202.
- S. Makhseed, M. Machacek, W. Alfadly, A. Tuhl, M. Vinodh, T. Simunek, V. Novakova, P. Kubat, E. Rudolf and P. Zimcik, *Chem. Commun.*, 2013, **49**, 11149-11151; H. He, P. C. Lo and D. K. P. Ng, *Chem – Eur. J.*, 2014, **20**, 6241-6245; H. J. Yoon and W.-D. Jang, *J. Porphyrins Phthalocyanines*, 2013, **17**, 16-26; M. P. Donzello, E. Viola, C. Ercolani, Z. Fu, D. Futur and K. M. Kadish, *Inorg. Chem.*, 2012, **51**, 12548-12559; F. Mitzel, S. FitzGerald, A. Beeby and R. Faust, *Eur. J. Org. Chem.*, 2004, 1136-1142; M. Machacek, A. Cidlina, V. Novakova, J. Svec, E. Rudolf, M. Miletin, E. Kučera, T. Simunek and P. Zimcik, *J. Med. Chem.*, 2015, **58**, 1736-1749.
- P. Löser, A. Winzenburg and R. Faust, *Chem. Commun.*, 2013, **49**, 9413-9415.
- J. Mosinger, K. Lang, P. Kubat, J. Sýkora, M. Hof, L. Plíštil and B. Mosinger, Jr., *J. Fluoresc.*, 2009, **19**, 705-713.
- I. V. Nesterova, S. S. Erdem, S. Pakhomov, R. P. Hammer and S. A. Soper, *J. Am. Chem. Soc.*, 2009, **131**, 2432-2433; I. V. Nesterova, C. A. Bennett, S. S. Erdem, R. P. Hammer, P. L. Deininger and S. A. Soper, *Analyst*, 2011, **136**, 1103-1105.
- V. Novakova, L. Lochman, I. Zajícová, K. Kopecky, M. Miletin, K. Lang, K. Kirakci and P. Zimcik, *Chem. – Eur. J.*, 2013, **19**, 5025-5028; V. Novakova, M. Miletin, K. Kopecky and P. Zimcik, *Chem. – Eur. J.*, 2011, **17**, 14273-14282.
- B. S. Erdoğan, D. Atilla, A. G. Gürek and V. Ahsen, *J. Porphyrins Phthalocyanines*, 2014, **18**, 139-148; L. Tsuchi, T. Nakagaki, M. Shimizu, E. Itoh, M. Yasutake and K. Ohta, *J. Porphyrins Phthalocyanines*, 2013, **17**, 1080-1093.
- M. V. Martínez-Díaz, G. de la Torre and T. Torres, *Chem. Commun.*, 2010, **46**, 7090-7108.
- M. E. Ragoussi, M. Ince and T. Torres, *Eur. J. Org. Chem.*, 2013, **2013**, 6475-6489.
- M. García-Iglesias, K. Peuntinger, A. Kahnt, J. Krausmann, P. Vázquez, D. González-Rodríguez, D. M. Guldí and T. Torres, *J. Am. Chem. Soc.*, 2013, **135**, 19311-19318.
- N. Kobayashi, H. Ogata, N. Nonaka and E. A. Luk'yanets, *Chem. – Eur. J.*, 2003, **9**, 5123-5134.
- N. Kobayashi, S. I. Nakajima, H. Ogata and T. Fukuda, *Chem. – Eur. J.*, 2004, **10**, 6294-6312.
- P. Zimcik, V. Novakova, K. Kopecky, M. Miletin, R. Z. Uslu Kobak, E. Svandřliková, L. Váchová and K. Lang, *Inorg. Chem.*, 2012, **51**, 4215-4223.
- K. Kopecky, V. Novakova, M. Miletin, R. Kucera and P. Zimcik, *Bioconjugate Chem.*, 2010, **21**, 1872-1879.
- V. N. Nemykin and E. A. Lukyanets, *Arkivoc*, 2010, 136-208.
- J. Xu, J. Chen, L. Chen, R. Hu, S. Q. Wang, S. Y. Li, J. S. Ma and G. Q. Yang, *Dyes Pigm.*, 2014, **109**, 144-150; M. J. Cook, A. J. Dunn, S. D. Howe, A. J. Thomson and K. J. Harrison, *J. Chem. Soc., Perkin Trans. 1*, 1988, 2453-2458.
- S. Makhseed, F. Ibrahim, J. Samuel, M. Helliwell, J. E. Warren, C. G. Bezzu and N. B. McKeown, *Chem. – Eur. J.*, 2008, **14**, 4810-4815; M. P. Donzello, G. De Mori, E. Viola, C. Ercolani, E. Bodo, L. Mannina, D. Capitani, C. Rizzoli, L. Gontrani, G. Aquilanti, K. M. Kadish and P. D'Angelo, *Inorg. Chem.*, 2011, **50**, 12116-12125.
- S. V. Kudrevich and J. E. Van Lier, *Can. J. Chem.*, 1996, **74**, 1718-1723.
- F. Mitzel, S. FitzGerald, A. Beeby and R. Faust, *Chem. Commun.*, 2001, 2596-2597.
- Z. Musil, P. Zimcik, M. Miletin, K. Kopecky and J. Lenco, *Eur. J. Org. Chem.*, 2007, 4535-4542.
- C. J. Song, C. K. Jang, W. Yao and J. Y. Jaung, *J. Chem. Res.*, 2013, **37**, 268-272.
- E. A. Lukyanets and V. N. Nemykin, *J. Porphyrins Phthalocyanines*, 2010, **14**, 1-40; V. N. Nemykin and E. A. Lukyanets, in *Handbook of Porphyrin Science*, eds. K. M. Kadish, K. M. Smith and R. Guilard, World Scientific, Singapore, 2010, vol. 3, pp. 1-323.
- V. Chauke and T. Nyokong, *Inorg Chim. Acta*, 2010, **363**, 3662-3669; I. Gurol, M. Durmus, V. Ahsen and T. Nyokong, *Dalton Trans.*, 2007, 3782-3791.
- J. C. Hazelton, B. Iddon, H. Suschitzky and L. H. Woolley, *J. Chem. Soc., Perkin Trans. 1*, 1992, 685-691; R. Garner, G. V. Garner and H. Suschitzky, *J. Chem. Soc. C*, 1970, 825-829; J. C. Hazelton, B. Iddon, H. Suschitzky and L. H. Woolley, *Tetrahedron*, 1995, **51**, 10771-10794.
- C. Rager, G. Schmid and M. Hanack, *Chem. – Eur. J.*, 1999, **5**, 280-288; V. N. Nemykin, S. V. Dudkin, F. Dumoulin, C. Hirel, A. G. Gurek and V. Ahsen, *Arkivoc*, 2014, 142-204.
- E. H. Mørkved, L. T. Holmaas, H. Kjösen and G. Hvistendahl, *Acta Chem. Scand.*, 1996, **50**, 1153-1156; P. Zimcik, M. Miletin, M. Kostka, J. Schwarz, Z. Musil and K. Kopecky, *J. Photochem. Photobiol., A*, 2004, **163**, 21-28.
- V. Novakova, M. Miletin, T. Filandrova, J. Lenčo, A. Růžička and P. Zimcik, *J. Org. Chem.*, 2014, **79**, 2082-2093.
- T. Fukuda and N. Kobayashi, in *Handbook of Porphyrin Science*, eds. K. M. Kadish, K. M. Smith and R. Guilard, World Scientific Publishing, Singapore, 2010, vol. 9., pp. 1-650.
- M. P. Donzello, G. De Mori, E. Viola, C. Ercolani, G. Ricciardi and A. Rosa, *Inorg. Chem.*, 2014, **53**, 8009-8019.
- F. Mitzel, S. FitzGerald, A. Beeby and R. Faust, *Chem. – Eur. J.*, 2003, **9**, 1233-1241; S. Vagin and M. Hanack, *Eur. J. Org. Chem.*, 2003, **2003**, 2661-2669.
- J. Mack and M. J. Stillman, in *The Porphyrin Handbook*, eds. K. M. Kadish, K. M. Smith and R. Guilard, Academic Press, San Diego, USA, 2003, vol. 16, pp. 43-116; J. Mack, N. Kobayashi and M. J. Stillman, *J. Porphyrins Phthalocyanines*, 2006, **10**, 1219-1237.
- M. Gouterman, *J. Mol. Spectrosc.*, 1961, **6**, 138-163.
- V. N. Nemykin, R. G. Hadt, R. V. Belosludov, H. Mizuseki and Y. Kawazoe, *J. Phys. Chem. A*, 2007, **111**, 12901-12913.
- V. N. Nemykin and R. G. Hadt, *J. Phys. Chem. A*, 2010, **114**, 12062-12066.
- M. Hanack and M. Lang, *Adv. Mater.*, 1994, **6**, 819-833; N. B. Chaure, J. L. Sosa-Sanchez, A. N. Cammidge, M. J. Cook and A. K. Ray, *Org. Electron.*, 2010, **11**, 434-438.

- 37 S. E. Maree and T. Nyokong, *J. Porphyrins Phthalocyanines*, 2001, **5**, 782-792.
- 38 K. Kameyama, M. Morisue, A. Satake and Y. Kobuke, *Angew. Chem., Int. Ed.*, 2005, **44**, 4763-4766.
- 39 V. Novakova, P. Zimcik, K. Kopecky, M. Miletin, J. Kuneš and K. Lang, *Eur. J. Org. Chem.*, 2008, **2008**, 3260-3263.
- 40 D. A. Fernández, J. Awruch and L. E. Dixelio, *Photochem. Photobiol.*, 1996, **63**, 784-792.
- 41 M. T. M. Choi, P. P. S. Li and D. K. P. Ng, *Tetrahedron*, 2000, **56**, 3881-3887.
- 42 R. W. Redmond and J. N. Gamlin, *Photochem. Photobiol.*, 1999, **70**, 391-475.
- 43 N. A. Kuznetsova and O. L. Kaliya, *J. Porphyrins Phthalocyanines*, 2012, **16**, 705-712.
- 44 G. Schnurpfeil, A. K. Sobbi, W. Spiller, H. Kliesch and D. Wöhrle, *J. Porphyrins Phthalocyanines*, 1997, **1**, 159-167.
- 45 M. P. Donzello, Z. Ou, D. Dini, M. Meneghetti, C. Ercolani and K. M. Kadish, *Inorg. Chem.*, 2004, **43**, 8637-8648; C. Bergami, M. P. Donzello, F. Monacelli, C. Ercolani and K. M. Kadish, *Inorg. Chem.*, 2005, **44**, 9862-9873.
- 46 G. De Mori, Z. Fu, E. Viola, X. H. Cai, C. Ercolani, M. P. Donzello and K. M. Kadish, *Inorg. Chem.*, 2011, **50**, 8225-8237; C. Bergami, M. P. Donzello, C. Ercolani, F. Monacelli, K. M. Kadish and C. Rizzoli, *Inorg. Chem.*, 2005, **44**, 9852-9861.
- 47 Z. P. Ou, Z. Jiang, N. S. Chen, J. L. Huang, J. Shen and K. M. Kadish, *J. Porphyrins Phthalocyanines*, 2008, **12**, 1123-1133.
- 48 A. Cidlina, V. Novakova, M. Miletin and P. Zimcik, *Dalton Trans.*, 2015, **44**, 6961-6971.
- 49 D. W. Clack, N. S. Hush and I. S. Woolsey, *Inorg. Chim. Acta*, 1976, **19**, 129-132.
- 50 E. Viola, M. P. Donzello, S. Ciattini, G. Portalone and C. Ercolani, *Eur. J. Inorg. Chem.*, 2009, **2009**, 1600-1607.
- 51 K. Kopecky, V. Novakova, M. Miletin, R. Kucera and P. Zimcik, *Tetrahedron*, 2011, **67**, 5956-5963.
- 52 X. J. Jiang, P. C. Lo, Y. M. Tsang, S. L. Yeung, W. P. Fong and D. K. P. Ng, *Chem. – Eur. J.*, 2010, **16**, 4777-4783.
- 53 P. Zimcik, M. Miletin, V. Novakova, K. Kopecky, M. Nejedla, V. Stara and K. Sedlackova, *Austr. J. Chem.*, 2009, **62**, 425-433.
- 54 V. Novakova, P. Zimcik, M. Miletin, K. Kopecky and Z. Musil, *Eur. J. Org. Chem.*, 2010, **2010**, 732-739.
- 55 M. Kostka, P. Zimcik, M. Miletin, P. Klemra, K. Kopecky and Z. Musil, *J. Photochem. Photobiol., A*, 2006, **178**, 16-25.
- J. Y. Jaung, K. Fukunishi and M. Matsuoka, *J. Heterocycl. Chem.*, 1997, **34**, 653-657.